Appl. Math. Mech. -Engl. Ed., **39**(9), 1341–1352 (2018)

Applied Mathematics and Mechanics (English Edition)

https://doi.org/10.1007/s10483-018-2366-9

Investigation of Coulomb force effects on ethylene glycol based nanofluid laminar flow in a porous enclosure*

M. SHEIKHOLESLAMI†

Department of Mechanical Engineering, Babol Noshirvani University of Technology, Babol 47148-71167, Iran

(Received Jan. 16, 2018 / Revised Mar. 22, 2018)

Abstract Forced convection heat transfer of ethylene glycol based nanofluid with Fe_3O_4 inside a porous medium is studied using the electric field. The control volume based finite element method (CVFEM) is selected for numerical simulation. The impact of the radiation parameter (R_d), the supplied voltage ($\Delta\varphi$), the volume fraction of nanofluid (ϕ), the Darcy number (Da), and the Reynolds number (Re) on nanofluid treatment is demonstrated. Results prove that thermal radiation increases the temperature gradient near the positive electrode. Distortion of isotherms increases with the enhance of the Darcy number and the Coulomb force.

Key words control volume based finite element method (CVFEM), porous medium, Coulomb force, nanofluid, thermal radiation, electric field

Chinese Library Classification O361
2010 Mathematics Subject Classification 76W05

Nomenclature

E_x, E_y, components of electric field;
D_e, diffusion number;
S_E, Lorentz force number;
u, v, components of velocity;
q, electric charge density;
J, electric current density;
p, pressure;
K, permeability of porous media;
T, temperature;
T_C, Curie temperature;
F_E, electric force;
Re, Reynolds number;
Da, Darcy number;
R_d, radiation parameter;
Pr_E, electric Prandtl number;
N_E, electric field number;
D, charge diffusion coefficient;
V, velocity;
k, thermal conductivity;
C_p, heat capacity;
q_r, radiation heat flux;
m, shape factor.

Greek symbols

ϕ, volume fraction;
σ, electric conductivity;
φ, potential electric field;
ε, dielectric permittivity;
ρ, density;
μ, dynamic viscosity;

* Citation: SHEIKHOLESLAMI, M. Investigation of Coulomb force effects on ethylene glycol based nanofluid laminar flow in a porous enclosure. *Applied Mathematics and Mechanics* (*English Edition*), **39**(9), 1341–1352 (2018) https://doi.org/10.1007/s10483-018-2366-9

† Corresponding author, E-mail: mohsen.sheikholeslami@yahoo.com

β_r, radiation coefficient;

σ_e, stefan Boltzmann coefficient.

Subscripts

s, solid particles;

f, base fluid;

c, cold;

nf, nanofluid;

h, hot.

1 Introduction

Nanofluid can be offered as an applicable way to improve heat transfer. Nanofluid convective simulation has been investigated by different researchers[1–5]. Sheikholeslami and Sadoughi[6] reported nanofluid convective flow in existence of melting surface. Sheikholeslami and Rokni[7] published a review article about various applications of magnetic nanofluid. A comprehensive review paper was published by Sheikholeslami and Ganji[8] to show importance of nanotechnology. The influence of radiation mode was examined by Hayat et al.[9]. The effect of Coulomb forces on nanofluid behavior was demonstrated by Sheikholeslami and Chamkha[10]. Their outputs revealed that the electric field is highly sensible in lower Reynolds numbers. Hassan et al.[11] showed an innovative model for predicting solar radiation. Nayak et al.[12] reported the roles of nanofluid radiative heat transfer.

The effect of shape factor on nanofluid properties was considered by Sheikholeslami and Bhatti[13]. Tao and He[14] presented free convection of nanofluid in an energy storage system. Makinde et al.[15] demonstrated the nanofluid flow considering non-uniform viscosity. Mezrhab et al.[16] reported the radiation impact in an enclosure. Sheremet et al.[17] illustrated the transient ferrofluid flow in a cavity by means of the finite difference method. Some researchers also used nanofluid as effective working fluid[18–41].

This research aims to model the effects of thermal radiation on nanofluid behavior in existence of Coulomb forces. The roles of Darcy number, radiation parameter, supplied voltage, volume fraction of nanofluid, and Reynolds number are demonstrated in results.

2 Problem statement

The ethylene glycol-Fe_3O_4 nanofluid is utilized. All walls are stationary except for the bottom wall. Figure 1 demonstrates a sample element and geometry. The influence of Re and Da on contour of q is demonstrated in Fig. 2. The effect of Re on q is less sensible than Da. As the Darcy number augments, the shape of isoelectric density lines becomes more complex.

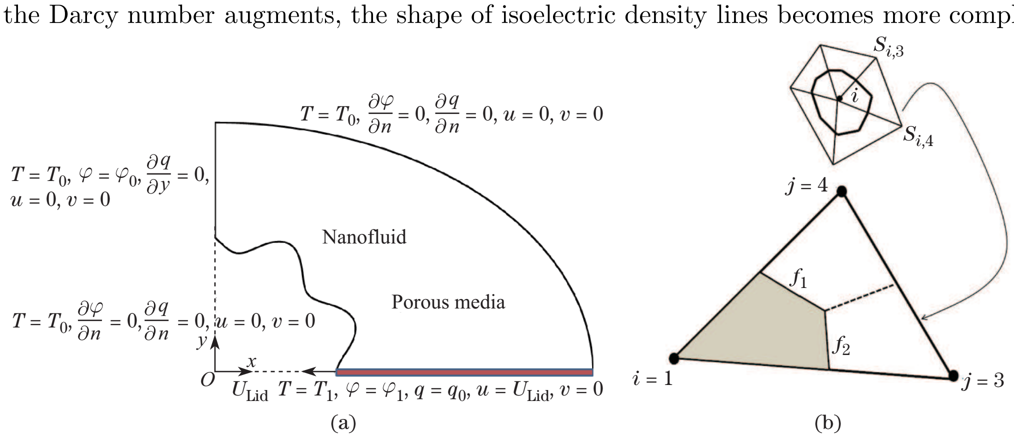

Fig. 1 (a) Geometry and boundary conditions and (b) a sample triangular element and its corresponding control volume

3 Governing formula and modeling

3.1 Governing formula

The definition of electric field is[23]

$$E = -\nabla\varphi, \tag{1}$$

$$q = \nabla\cdot\varepsilon E, \tag{2}$$

$$J = qV - D\nabla q + \sigma E, \tag{3}$$

$$\nabla\cdot J + \frac{\partial q}{\partial t} = 0. \tag{4}$$

The governing formulae are[23]

$$\begin{cases} \nabla\cdot V = 0, \\ \dfrac{qE}{\rho_{\rm nf}} - \dfrac{\mu_{\rm nf}}{K\rho_{\rm nf}}V + \dfrac{\mu_{\rm nf}}{\rho_{\rm nf}}\nabla^2 V - \dfrac{\nabla p}{\rho_{\rm nf}} = \Big((V\cdot\nabla)V + \dfrac{\partial V}{\partial t}\Big), \\ \Big((V\cdot\nabla)T + \dfrac{\partial T}{\partial t}\Big) = \dfrac{k_{\rm nf}}{(\rho C_p)_{\rm nf}}\nabla^2 T - \dfrac{1}{(\rho C_p)_{\rm nf}}\dfrac{\partial q_{\rm r}}{\partial y} + \dfrac{J\cdot E}{(\rho C_p)_{\rm nf}}, \\ T^4 \cong 4T_{\rm C}^3 T - 3T_{\rm C}^4, \quad q_{\rm r} = -\dfrac{4\sigma_{\rm e}}{3\beta_{\rm r}}\dfrac{\partial T^4}{\partial y}, \\ \nabla\varphi = -E, \quad q = \nabla\cdot\varepsilon E, \quad \dfrac{\partial q}{\partial t} = -\nabla\cdot J. \end{cases} \tag{5}$$

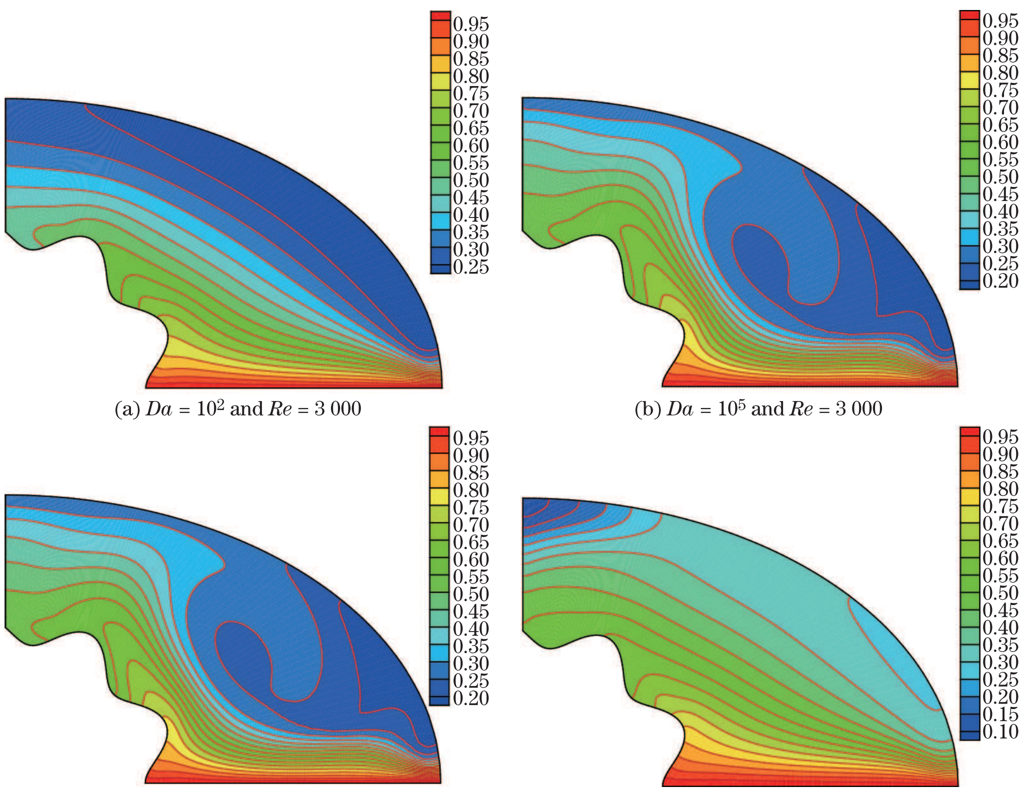

(a) $Da = 10^2$ and $Re = 3\,000$

(b) $Da = 10^5$ and $Re = 3\,000$

(c) $Da = 10^2$ and $Re = 6\,000$

(d) $Da = 10^5$ and $Re = 6\,000$

Fig. 2 Electric density distributions injected by the bottom electrode when $\Delta\varphi = 10\,\text{kV}$, $\phi = 0.05$, and $R_{\rm d} = 0.8$ (color online)

$(\rho C_p)_{\mathrm{nf}}$, μ_{nf}, and ρ_{nf} are[26]

$$\begin{cases} (\rho C_p)_{\mathrm{nf}} = (\rho C_p)_{\mathrm{s}}\varphi + (1-\phi)(\rho C_p)_{\mathrm{f}}, \\ \mu = A_1 + A_2(\Delta\varphi) + A_3(\Delta\varphi)^2 + A_4(\Delta\varphi)^3, \\ \rho_{\mathrm{nf}} = \rho_{\mathrm{f}}(1-\phi) + \rho_{\mathrm{s}}\phi. \end{cases} \tag{6}$$

Properties of Fe_3O_4 and $C_2H_6O_2$ are illustrated in Table 1[26]. Table 2 shows the coefficient values of A_i $(i=1,2,3,4)$[7]. k_{nf} can be obtained from

$$\frac{k_{\mathrm{nf}}}{k_{\mathrm{f}}} = \frac{-m(k_{\mathrm{f}}-k_{\mathrm{p}})\phi + (k_{\mathrm{p}}-k_{\mathrm{f}})\phi + mk_{\mathrm{f}} + k_{\mathrm{p}} + k_{\mathrm{f}}}{mk_{\mathrm{f}} + (k_{\mathrm{f}}-k_{\mathrm{p}})\phi + k_{\mathrm{f}} + k_{\mathrm{p}}}. \tag{7}$$

Table 3 depicts various shape factors.

Table 1 Thermo physical properties of ethylene glycol and nanoparticles

	$\rho/(\mathrm{kg\cdot m^{-3}})$	$C_p/(\mathrm{J\cdot kg^{-1}\cdot K^{-1}})$	$k/(\mathrm{W\cdot m^{-1}\cdot K^{-1}})$
Ethylene glycol	1 110	2 400	0.26
Fe_3O_4	5 200	670	6

Table 2 Coefficient values of Eq. (6)

Coefficient value	$\phi = 0$	$\phi = 0.05$
A_1	$1.060\,3\times10^{1}$	9.533 1
A_2	-2.698×10^{-3}	$-3.411\,9\times10^{-3}$
A_3	$2.908\,2\times10^{-6}$	$5.522\,8\times10^{-6}$
A_4	$-1.187\,6\times10^{-8}$	$-4.134\,4\times10^{-8}$

Table 3 Values of shape factor of different shapes of nanoparticles

m	Spherical		3.0
	Platelet		5.7
	Cylinder		4.8
	Brick	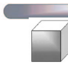	3.7

Therefore, the final partial differential equations are

$$\begin{cases} \nabla\cdot V = 0, \\ \Big((V\cdot\nabla)V + \dfrac{\partial V}{\partial t}\Big) = \dfrac{1}{Re}\dfrac{\rho_{\mathrm{nf}}/\rho_{\mathrm{f}}}{\mu_{\mathrm{nf}}/\mu_{\mathrm{f}}}\nabla^2 V - \nabla p + \dfrac{S_{\mathrm{E}}}{\rho_{\mathrm{nf}}/\rho_{\mathrm{f}}}qE - \dfrac{1}{Re\,Da}\dfrac{\mu_{\mathrm{nf}}}{\mu_{\mathrm{f}}}\Big(\dfrac{\rho_{\mathrm{nf}}}{\rho_{\mathrm{f}}}\Big)^{-1}V, \\ \Big((V\cdot\nabla)\theta + \dfrac{\partial\theta}{\partial t}\Big) = \dfrac{1}{PrRe}\dfrac{k_{\mathrm{nf}}/k_{\mathrm{f}}}{(\rho C_p)_{\mathrm{nf}}/(\rho C_p)_{\mathrm{f}}}\nabla^2\theta + \dfrac{4}{3}\Big(\dfrac{k_{\mathrm{nf}}}{k_{\mathrm{f}}}\Big)^{-1}R_{\mathrm{d}}\dfrac{\partial^2\theta}{\partial Y^2} \\ + S_{\mathrm{E}}\dfrac{1}{(\rho C_p)_{\mathrm{nf}}/(\rho C_p)_{\mathrm{f}}}Ec(J\cdot E), \\ E = -\nabla\varphi, \quad q = \nabla\cdot\varepsilon E, \quad \nabla\cdot J = -\dfrac{\partial q}{\partial t}, \end{cases} \tag{8}$$

where

$$\begin{cases} (\overline{u},\overline{v}) = \dfrac{(u,v)}{U_{\mathrm{Lid}}}, \quad \overline{\varphi} = \dfrac{\varphi-\varphi_0}{\nabla\varphi}, \quad (\overline{y},\overline{x}) = \dfrac{(y,x)}{L}, \quad \theta = \dfrac{T-T_0}{\nabla T}, \\ \overline{t} = \dfrac{tU_{\mathrm{Lid}}}{L}, \quad \overline{p} = \dfrac{P}{\rho U_{\mathrm{Lid}}^2}\overline{q} = \dfrac{q}{q_0}, \quad \overline{E} = \dfrac{E}{E_0}, \\ \nabla T = T_1 - T_0, \quad \nabla\varphi = \varphi_1 - \varphi_0. \end{cases} \tag{9}$$

Ψ and Ω are employed in order to diminish the pressure gradient,

$$v = -\frac{\partial \psi}{\partial x}, \quad \omega = \frac{\partial v}{\partial x} - \frac{\partial u}{\partial y}, \quad \frac{\partial \psi}{\partial y} = u, \quad \Psi = \frac{\psi L}{U_{\mathrm{Lid}}}, \quad \Omega = \frac{\omega}{L U_{\mathrm{Lid}}}. \tag{10}$$

The local Nusselt number Nu_{loc} and the average Nusselt number Nu_{ave} over the bottom wall are

$$Nu_{\mathrm{loc}} = \Big(\frac{k_{\mathrm{nf}}}{k_{\mathrm{f}}}\Big)\Big(1 + \frac{4}{3} R_{\mathrm{d}} \Big(\frac{k_{\mathrm{nf}}}{k_{\mathrm{f}}}\Big)^{-1}\Big)\frac{\partial \Theta}{\partial Y}, \tag{11}$$

$$Nu_{\mathrm{ave}} = \frac{1}{L}\int_{r_{\mathrm{in}}}^{r_{\mathrm{out}}} Nu_{\mathrm{loc}} \mathrm{d}x. \tag{12}$$

3.2 CVFEM

In order to estimate scalars, we utilize linear interpolation in the triangular element (see Fig. 1(b)). A Gauss-Seidel tool is employed to obtain the final answer after discretization[29].

4 Mesh study and code validation

Various mesh sizes are tested to find the independent result of the mesh. Table 4 demonstrates an example. This table indicates that the size of 81×241 can be selected. The CVFEM code is validated by comparing the results with those published in Refs. [23] and [25] (see Fig. 3). Good agreement can be found.

Table 4 Comparison of Nu_{ave} along lid wall for different grid resolutions at $R_{\mathrm{d}} = 0.8$, $Re = 6\,000$, $Da = 10^5$, $\Delta\varphi = 10\,\mathrm{kV}$, $\phi = 0.05$, and $Pr = 6.8$

Size	51×151	61×181	71×211	81×241	91×271	101×301
Nu_{ave}	6.299 867	6.307 856	6.309 132	6.318 96	6.319 06	6.319 87

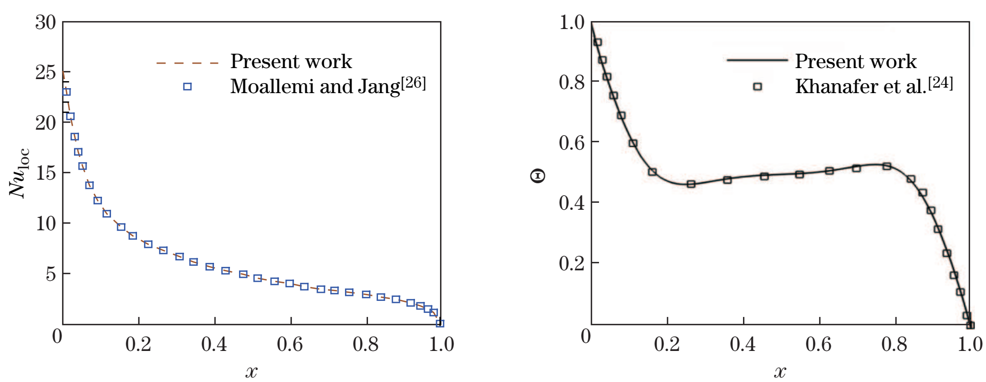

Fig. 3 (a) Comparison of the local Nusselt number over the lid wall between the present results and numerial results of Moallemi and Jang[26] at $Re = 500$, $R_{\mathrm{d}} = 0.4$, and $Pr = 1$; (b) comparison of the average Nusselt number between the present results and numerical results of Khanafer et al.[24] at $Gr = 10^4$, $\phi = 0.1$, and $Pr = 6.8$ (Cu-water)

5 Results and discussion

Electrohydrodynamic nanofluid forced convection in presence of thermal radiation is reported. The porous enclosure is filled with Fe_3O_4-ethylene glycol and has one lid wall. Roles of the Darcy number ($Da = 10^2$ to 10^5), the supplied voltage ($\Delta\varphi = 0\,\mathrm{kV}$ to $10\,\mathrm{kV}$), the volume fraction of Fe_3O_4 ($\phi = 0\%$ to 5%), the radiation parameter ($R_{\mathrm{d}} = 0$ to 0.8), and the Reynolds number ($Re = 3\,000$ to $6\,000$) are illustrated graphically.

At first, the impact of the shape factor on the rate of heat transfer is reported in Table 5. In this table, various shapes of nanoparticles are utilized. The maximum Nu happens by platelet. Therefore, platelet nanoparticles are utilized for more investigation.

Table 5 Effect of shape of nanoparticles on the Nusselt number when $R_{\mathrm{d}} = 0.8, Re = 6\,000, \Delta\varphi = 10\,\mathrm{kV}$, and $\phi = 0.05$

Shape	Da	
	10^2	10^5
Spherical	3.697 271	6.084 579
Brick	3.740 571	6.147 401
Cylinder	3.805 097	6.239 713
Platelet	3.855 149	6.318 966

Figures 4–7 depict the impacts of Da, Re, and $\Delta\varphi$ on isotherms and streamlines. At low Re, there is one clockwise vortex in streamline. The midpoint of main vortex is near the positive electrode. Augmenting the Darcy number leads to generation of the second eddy which rotates counter clockwise and the center of main eddy shift to upper side. Applying the electric field causes the strength of the main vortex to enhance and shift the midpoint of the eddy to upper side. Isotherms become more disturbed when $\Delta\varphi \neq 0\,\mathrm{kV}$. Thermal plume appears by increasing the Reynolds number. Also, by augmenting Re, $\psi_{\max}$ augments. As the Coulomb force increases, the secondary eddy diminishes and the strength of main eddy enhances.

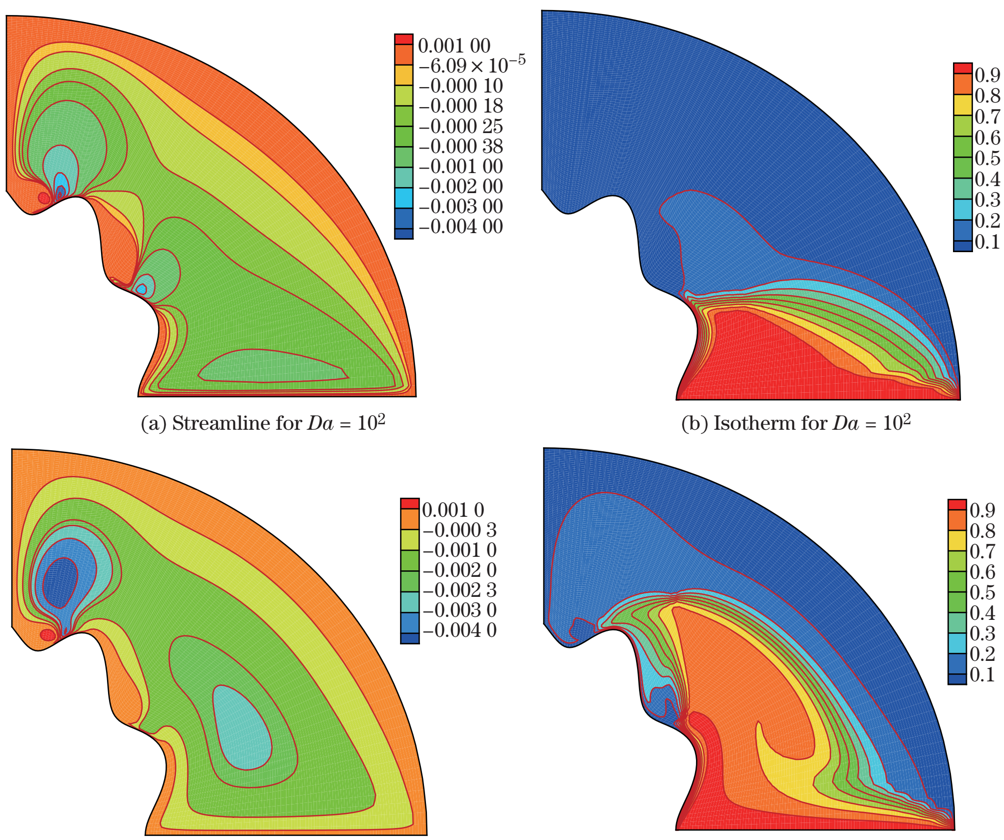

(a) Streamline for $Da = 10^2$ (b) Isotherm for $Da = 10^2$

(c) Streamline for $Da = 10^5$ (d) Isotherm for $Da = 10^5$

Fig. 4 Effects of Darcy number on streamlines and isotherms when $Re = 3\,000$, $\Delta\varphi = 0\,\mathrm{kV}$, $\phi = 0.05$, and $R_{\mathrm{d}} = 0.8$ (color online)

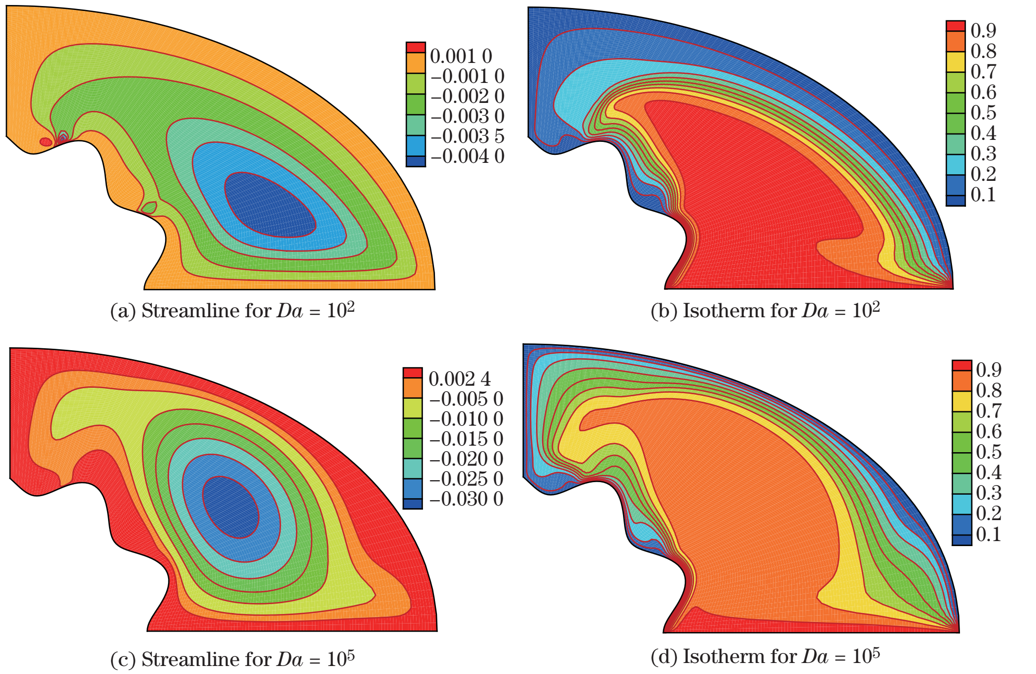

Fig. 5 Effects of Darcy number on streamlines and isotherms when $Re = 3\,000$, $\Delta\varphi = 10\,\mathrm{kV}$, $\phi = 0.05$, and $R_{\mathrm{d}} = 0.8$ (color online)

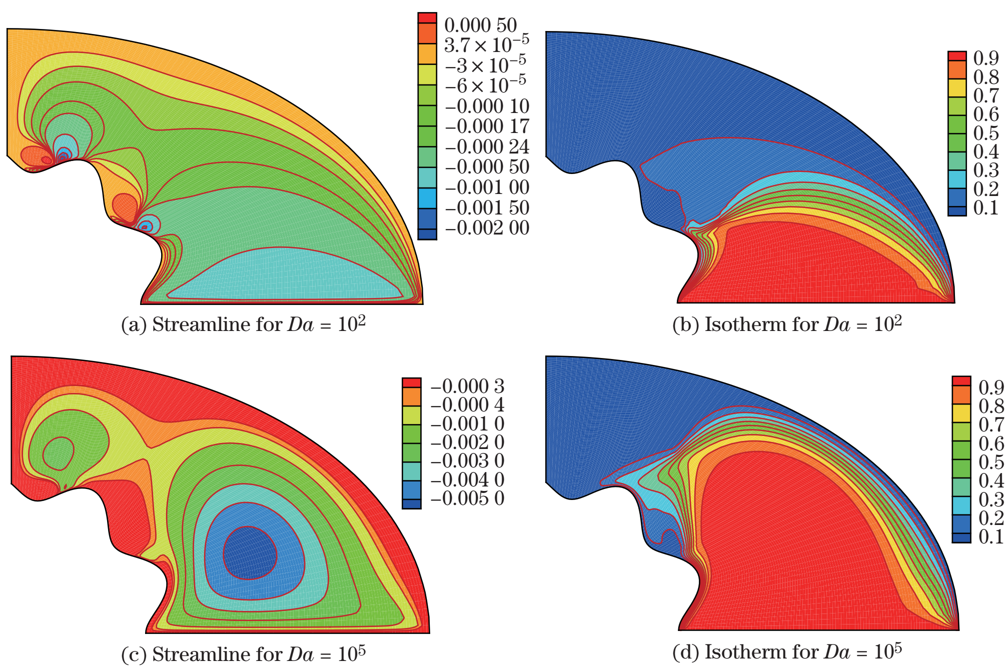

Fig. 6 Effects of Darcy number on streamlines and isotherms when $Re = 6\,000$, $\Delta\varphi = 0\,\mathrm{kV}$, $\phi = 0.05$, $R_{\mathrm{d}} = 0.8$ (color online)

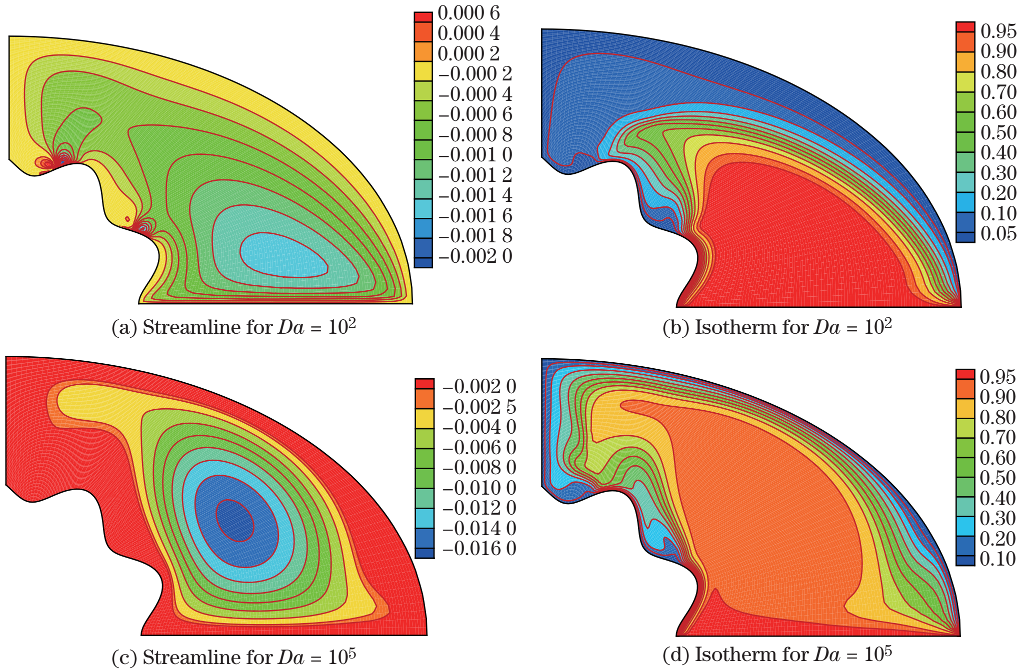

Fig. 7 Effects of Darcy number on streamlines and isotherms when $Re = 6\,000$, $\Delta\varphi = 10\,\text{kV}$, $\phi = 0.05$, $R_{\rm d} = 0.8$ (color online)

$Nu_{\rm ave}$ versus $Re, Da, R_{\rm d}$, and $\Delta\varphi$ is depicted in Fig. 8. The related formula is

$$\begin{aligned} Nu_{\rm ave} = & -2.26 + 0.08\Delta\varphi + 2.01Re^* + 1.05\,\lg\,Da + 3.25R_{\rm d} \\ & - 0.036\Delta\varphi Re^* + 0.023\Delta\varphi\,\lg\,Da \\ & + 0.15\Delta\varphi R_{\rm d} - 0.31Re^*\,\lg\,Da \\ & - 0.64Re^*R_{\rm d} + 0.41\,\lg\,DaR_{\rm d} \\ & + 0.015\Delta\varphi^2 - 0.2(Re^*)^2 - 0.14(\lg\,Da)^2 + 1.46R_{\rm d}^2, \end{aligned} \tag{13}$$

where $Re^* = 0.001Re$. In absence of the Coulomb force, the Nusselt number augments with the increase of Reynolds number, while an opposite behavior is reported in existence of such forces. The electric field helps the convective mode enhance. Therefore, $Nu_{\rm ave}$ augments with the increase of $\Delta\varphi$. Thermal radiation enhances the temperature gradient near the lid wall. The influence of Darcy number is the same as the radiation parameter. Therefore, $Nu_{\rm ave}$ is an increasing function of $R_{\rm d}$ and Da.

6 Conclusions

Forced convection and radiation of nanofluid inside a lid driven permeable media in existence of electric field are modeled. Outputs are reported for different values of Da, $R_{\rm d}$, ϕ, $\Delta\varphi$, and Re. Outputs demonstrate that the shape of isotherms becomes more complex with the augment of Da, $R_{\rm d}$, and Coulomb forces. Applying the electric field makes the secondary eddy to diminish. The temperature gradient enhances with the increase in the radiation parameter.

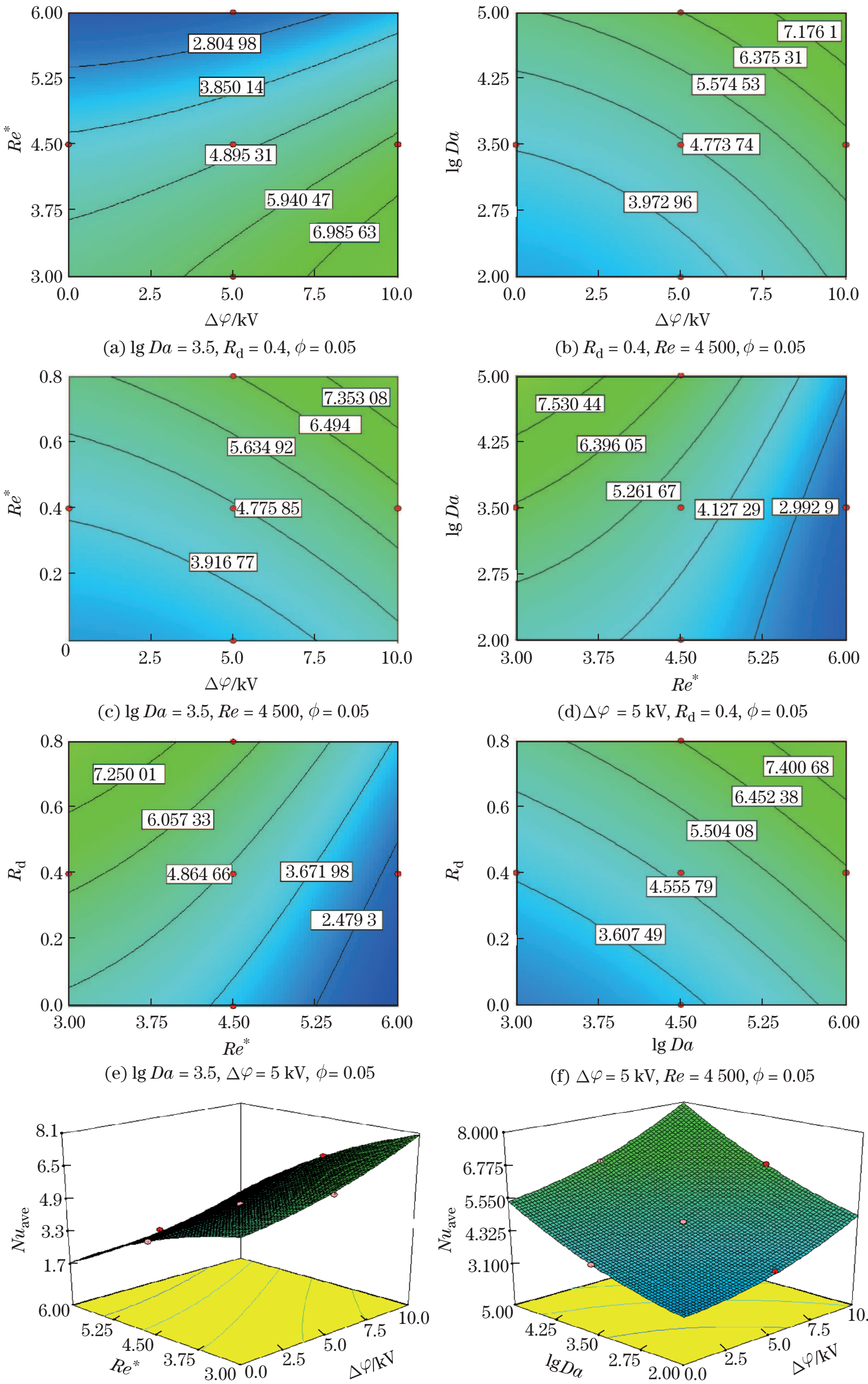

(a) lg Da = 3.5, R_d = 0.4, ϕ = 0.05

(b) R_d = 0.4, Re = 4 500, ϕ = 0.05

(c) lg Da = 3.5, Re = 4 500, ϕ = 0.05

(d) $\Delta\varphi$ = 5 kV, R_d = 0.4, ϕ = 0.05

(e) lg Da = 3.5, $\Delta\varphi$ = 5 kV, ϕ = 0.05

(f) $\Delta\varphi$ = 5 kV, Re = 4 500, ϕ = 0.05

(g) lg Da = 3.5, R_d = 0.4, ϕ = 0.05

(h) R_d = 0.4, Re = 4 500, ϕ = 0.05

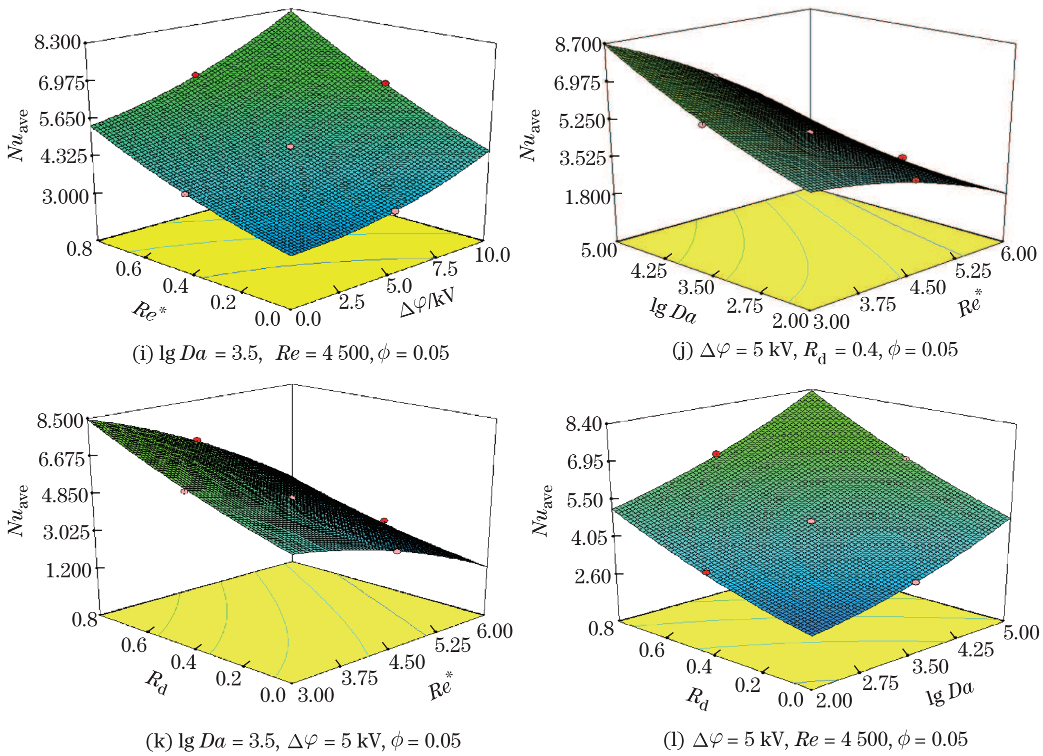

Fig. 8 Effects of Da, $\Delta\varphi$, R_{d}, and Re on average Nusselt number (color online)

References

[1] SHEIKHOLESLAMI, M., GANJI, D. D., ASHORYNEJAD, H. R., and ROKNI, H. B., Analytical investigation of Jeffery-Hamel flow with high magnetic field and nano particle by Adomian decomposition method. *Applied Mathematics and Mechanics* (*English Edition*), **33**(1), 25–36 (2012) https://doi.org/10.1007/s10483-012-1531-7

[2] SHEIKHOLESLAMI, M. and SHEHZAD, S. A. CVFEM simulation for nanofluid migration in a porous medium using Darcy model. *International Journal of Heat and Mass Transfer*, **122**, 1264–1271 (2018)

[3] SHEIKHOLESLAMI, M., GORJI-BANDPY, M., and DOMAIRRY, G. Free convection of nanofluid filled enclosure using lattice Boltzmann method (LBM). *Applied Mathematics and Mechanics* (*English Edition*), **34**(7), 833–846 (2013) https://doi.org/10.1007/s10483-013-1711-9

[4] MAPARU, A. K., GANVIR, V., and RAI, B. Titania nanofluids with improved photocatalytic activity under visible light. *Colloids and Surfaces A*: *Physicochemical and Engineering Aspects*, **482**, 345–352 (2015)

[5] SHEIKHOLESLAMI, M. and ROKNI, H. B. Magnetic nanofluid flow and convective heat transfer in a porous cavity considering Brownian motion effects. *Physics of Fluids*, **30**(1), 012003 (2018)

[6] SHEIKHOLESLAMI, M. and SADOUGHI, M. K. Simulation of CuO-water nanofluid heat transfer enhancement in presence of melting surface. *International Journal of Heat and Mass Transfer*, **116**, 909–919 (2018)

[7] SHEIKHOLESLAMI, M. and ROKNI, H. B. Simulation of nanofluid heat transfer in presence of magnetic field: a review. *International Journal of Heat and Mass Transfer*, **115**, 1203–1233 (2017)

[8] SHEIKHOLESLAMI, M. and GANJI, D. D. Nanofluid convective heat transfer using semi analytical and numerical approaches: a review. *Journal of the Taiwan Institute of Chemical Engineers*, **65**, 43–77 (2016)

[9] HAYAT, T., QAYYUM, S., IMTIAZ, M., and ALSAEDI, A. Comparative study of silver and copper water nanofluids with mixed convection and nonlinear thermal radiation. *International Journal of Heat and Mass Transfer*, **102**, 723–732 (2016)

[10] SHEIKHOLESLAMI, M. and CHAMKHA, A. J. Electrohydrodynamic free convection heat transfer of a nanofluid in a semi-annulus enclosure with a sinusoidal wall. *Numerical Heat Transfer, Part A*, **69**(7), 781–793 (2016)

[11] HASSAN, G. E., ELSAYED, M., ZAHRAA, E., ALI, M. A., and HANAFY, A. A. New temperature-based models for predicting global solar radiation. *Applied Energy*, **179**, 437–450 (2016)

[12] NAYAK, M. K., AKBAR, N. S., PANDEY, V. S., KHAN, Z. H., and TRIPATHI, D. 3D free convective MHD flow of nanofluid over permeable linear stretching sheet with thermal radiation. *Powder Technology*, **315**, 205–215 (2017)

[13] SHEIKHOLESLAMI, M. and BHATTI, M. M. Forced convection of nanofluid in presence of constant magnetic field considering shape effects of nanoparticles. *International Journal of Heat and Mass Transfer*, **111**, 1039–1049 (2017)

[14] TAO, Y. B. and HE, Y. L. Effects of natural convection on latent heat storage performance of salt in a horizontal concentric tube. *Applied Energy*, **143**, 38–46 (2015)

[15] MAKINDE, O. D., MABOOD, F., KHAN, W. A., and TSHEHLA, M. S. MHD flow of a variable viscosity nanofluid over a radially stretching convective surface with radiative heat. *Journal of Molecular Liquids*, **219**, 624–630 (2016)

[16] MEZRHAB, A., BOUALI, H., AMAOUI, H., and BOUZI, M. Computation of combined natural-convection and radiation heat-transfer in a cavity having a square body at its center. *Applied Energy*, **83**(9), 1004–1023 (2006)

[17] SHEREMET, M. A., POP, I., and ROŞA, N. C. Magnetic field effect on the unsteady natural convection in a wavy-walled cavity filled with a nanofluid: Buongiorno's mathematical model. *Journal of the Taiwan Institute of Chemical Engineers*, **61**, 211–222 (2016)

[18] HAYAT, T., NISAR, Z., YASMIN, H., and ALSAEDI, A. Peristaltic transport of nanofluid in a compliant wall channel with convective conditions and thermal radiation. *Journal of Molecular Liquids*, **220**, 448–453 (2016)

[19] RAJU, C. S. K., SANDEEP, N., and SUGUNAMMA, V. Unsteady magneto-nanofluid flow caused by a rotating cone with temperature dependent viscosity: a surgical implant application. *Journal of Molecular Liquids*, **222**, 1183–1191 (2016)

[20] AHMAD, R. and MUSTAFA, M. Model and comparative study for rotating flow of nanofluids due to convectively heated exponentially stretching sheet. *Journal of Molecular Liquids*, **220**, 635–641 (2016)

[21] CHAMKHA, A. J. and AHMED, S. E. Unsteady MHD stagnation-point flow with heat and mass transfer for a three-dimensional porous body in the presence of heat generation/absorption and chemical reaction. *Progress in Computational Fluid Dynamics*, **11**, 388–396 (2011)

[22] BACHOK, N., ISHAK, A., NAZAR, R., and POP, I. Flow and heat transfer at a general three-dimensional stagnation point in a nanofluid. *Physica B: Condensed Matter*, **405**(24), 4914–4918 (2010)

[23] HAYAT, T., KHAN, I. M., FAROOQ, M., ALSAEDI, A., and YASMEEN, T. Impact of Marangoni convection in the flow of carbon-water nanofluid with thermal radiation. *International Journal of Heat and Mass Transfer*, **106**, 810–815 (2017)

[24] KHANAFER, K., VAFAI, K., and LIGHTSTONE, M. Buoyancy-driven heat transfer enhancement in a two-dimensional enclosure utilizing nanofluids. *International Journal of Heat and Mass Transfer*, **446**, 3639–3653 (2003)

[25] SHEIKHOLESLAMI, M. *Application of Control Volume based Finite Element Method (CVFEM) for Nanofluid Flow and Heat Transfer*, 1st ed., Elsevier, Amsterdam (2018)

[26] MOALLEMI, M. K. and JANG, K. S. Prandtl number effects on laminar mixed convection heat transfer in a lid-driven cavity. *International Journal of Heat and Mass Transfer*, **35**, 1881–1892 (1992)

[27] RARANI, E. M., ETESAMI, N., and NASR ESFAHANY, M. Influence of the uniform electric field on viscosity of magnetic nanofluid (Fe_3O_4-EG). *Journal of Applied Physics*, **112**, 094903 (2012)

[28] CHAMKHA, A. J., ABD EL-AZIZ, M. M., and AHMED, S. E. Effects of thermal stratification on flow and heat transfer due to a stretching cylinder with uniform suction/injection. *International Journal of Energy and Technology*, **2**, 1–7 (2010)

[29] REHMAN, F. U., NADEEM, S., and HAQ, R. U. Heat transfer analysis for three-dimensional stagnation-point flow over an exponentially stretching surface. *Chinese Journal of Physics*, **55**, 1552–1560 (2017)

[30] RAEES, A., XU, H., SUN, Q., and POP, I. Mixed convection in a gravity-driven nano-liquid film containing both nanoparticles and gyrotactic microorganisms. *Applied Mathematics and Mechanics* (*English Edition*), **36**(2), 163–178 (2015) https://doi.org/10.1007/s10483-015-1901-7

[31] TAHIR, F., GUL, T., ISLAM, S., SHAH, Z., KHAN, A., KHAN, W., and ALI, W. Flow of a nano-liquid film of Maxwell fluid with thermal radiation and magneto hydrodynamic properties on an unstable stretching sheet. *Journal of Nanofluids*, **6**, 1021–1030 (2017)

[32] SOOMRO, F. A., HAQ, R. U., AL-MDALLAL, Q. M., and ZHANG, Q. Heat generation/absorption and nonlinear radiation effects on stagnation point flow of nanofluid along a moving surface. *Results in Physics*, **8**, 404–414 (2018)

[33] KHAN, N. S., GUL, T., ISLAM, S., KHAN, A., and SHAH, Z. Brownian motion and thermophoresis effects on MHD mixed convective thin film second-grade nanofluid flow with Hall effect and heat transfer past a stretching sheet. *Journal of Nanofluids*, **6**, 1–18 (2017)

[34] SHEIKHOLESLAMI, M. Numerical investigation for CuO-H_2O nanofluid flow in a porous channel with magnetic field using mesoscopic method. *Journal of Molecular Liquids*, **249**, 739–746 (2018)

[35] MIRZA, I. A., ABDULHAMEED, M., and SHAFIE, S. Magnetohydrodynamic approach of non-Newtonian blood flow with magnetic particles in stenosed artery. *Applied Mathematics and Mechanics* (*English Edition*), **38**(3), 379–392 (2017) https://doi.org/10.1007/s10483-017-2172-7

[36] HAYAT, T., NAZAR, H., IMTIAZ, M., and ALSAEDI, A. Darcy-Forchheimer flows of copper and silver water nanofluids between two rotating stretchable disks. *Applied Mathematics and Mechanics* (*English Edition*), **38**(12), 1663–1678 (2017) https://doi.org/10.1007/s10483-017-2289-8

[37] SHEHZAD, S. A., HAYAT, T., ALSAEDI, A., and MERAJ, M. A. Cattaneo-Christov heat and mass flux model for 3D hydrodynamic flow of chemically reactive Maxwell liquid. *Applied Mathematics and Mechanics* (*English Edition*), **38**(10), 1347–1356 (2017) https://doi.org/10.1007/s10483-017-2250-6

[38] AHMED, S. E. Modeling natural convection boundary layer flow of micropolar nanofluid over vertical permeable cone with variable wall temperature. *Applied Mathematics and Mechanics* (*English Edition*), **38**(8), 1171–1180 (2017) https://doi.org/10.1007/s10483-017-2231-9

[39] ZHAO, Q. K., XU, H., TAO, L. B., RAEES, A., and SUN, Q. Three-dimensional free bio-convection of nanofluid near stagnation point on general curved isothermal surface. *Applied Mathematics and Mechanics* (*English Edition*), **37**(4), 417–432 (2016) https://doi.org/10.1007/s10483-016-2046-9

[40] XU, H. A homogeneous-heterogeneous reaction model for heat fluid flow in the stagnation region of a plane surface. *International Communications in Heat and Mass Transfer*, **87**, 112–117 (2017)

[41] TURKYILMAZOGLU, M. Flow of nanofluid plane wall jet and heat transfer. *European Journal of Mechanics-B/Fluids*, **59**, 18–24 (2016)